

## Molecular Dynamics of DNA: Comparison of Force Fields and Terminal Nucleotide Definitions

Clarisse G. Ricci, Alex S. C. de Andrade, Melina Mottin, and Paulo A. Netz\*

Instituto de Química, Universidade Federal do Rio Grande do Sul, 91501-970 Porto Alegre, RS, Brazil

Received: April 20, 2010; Revised Manuscript Received: June 16, 2010

Despite DNA being a very important target for several proteins and drugs, molecular dynamics simulations with nucleic acids still encompass many challenges, such as the reliability of the chosen force field. In this paper, we carried out molecular dynamics simulations of the Dickerson–Drew dodecamer comparing GROMOS 53A6 and AMBER 03 force fields. While the AMBER force field presents specific topologies for the 5' and 3' terminal nucleotides, the GROMOS force field considers all nucleotides in the same way. To investigate the effects of the terminal nucleotide definitions, both force fields were modified to be applied in the two possible ways: with or without specific terminal nucleotide topologies. The analysis of global stability (rmsd, number of base pairs and hydrogen bonds) showed that both systems simulated with AMBER were stable, while the system simulated with the original GROMOS topologies was very unstable after 5 ns. When specific terminal topologies were included for GROMOS force field, DNA denaturation was delayed until 15 ns, but not avoided. The  $\alpha/\gamma$  transitions also displayed a strong dependence on the force field, but not on the terminal nucleotide definitions: AMBER simulations mainly explored configurations corresponding to the global minimum, while GROMOS simulations exhibited, very early in the simulations, an extensive sampling of local minima that may facilitate transitions to A-DNA isoform. The  $\varepsilon/\zeta$  sampling was dependent both on the force field and on the terminal nucleotide definitions: while the AMBER simulations displayed well-defined B-I  $\rightarrow$  B-II transitions, the GROMOS force field clearly favored the B-I conformation. Also, the system simulated with the original GROMOS topologies displayed uncoupled  $\varepsilon/\zeta$  transitions, leading to noncanonical conformations, but this was reverted when the new terminal nucleotide topologies were applied. Finally, the GROMOS force field leads to strong geometrical deformations on the DNA (overestimated groove widths and roll and strongly underestimated twist and slide), which restrict the use of GROMOS force field in long time scale DNA simulations unless a further reparametrization is made.

### Introduction

Very complex systems such as nucleic acids often require special approaches in order to understand some experimental results or to build models at the microscopic scale. Molecular dynamics simulations are among those special approaches and as such they have a long story built upon challenges.<sup>1–4</sup> Regarding nucleic acids simulation, the choice of an adequately representative fragment is the first challenge, because the conformations and structural peculiarities of DNA are strongly dependent on the sequence.<sup>5,6</sup> This structural variability plays an important biological role, since the interactions of proteins and ligands with DNA depend on the sequence in two ways: by direct readout of the interaction patterns and by means of an indirect, shape-dependent recognition.<sup>7–10</sup>

Since the DNA backbone conformation is defined by six different torsion angles (see Figure 1), it means that the available conformational space of nucleic acids is far more complex than the conformational space of proteins, thus requiring long simulation times to relax the DNA structure. Also, DNA exhibits charged phosphate groups which demand a very precise treatment for long-range electrostatic interactions, and a large surface-to-volume ratio that requires explicit treatment of the solvent and an accurate description of the ionic force. Altogether, these challenges are reflected by the rather small number of

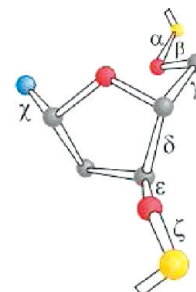


**Figure 1.** Backbone ( $\alpha$ ,  $\beta$ ,  $\gamma$ ,  $\delta$ ,  $\epsilon$ , and  $\zeta$ ) and glycosidic ( $\chi$ ) torsion angles, adapted from ref 12. Phosphorus atoms are depicted in yellow, oxygen atoms in red, carbon (united) atoms in gray, and nitrogen atoms in blue.

nucleic acids simulations compared with protein simulations, despite DNA being a very important biological target to many proteins and drugs.<sup>11</sup>

Hitherto, several force fields have been proposed to simulate biological molecules.<sup>3</sup> Among these, CHARMM,<sup>13–15</sup> AMBER,<sup>16–18</sup> GROMOS,<sup>19–22</sup> OPLS,<sup>23,24</sup> ENCAD,<sup>25</sup> and BMS<sup>26</sup> have been used in nucleic acids simulations. Although many studies compared the use of these different force fields in DNA simulations,<sup>27</sup> a critical analysis of their relative merits regarding long time scale DNA simulations is still missing in some cases.

In this paper, we chose two force fields, AMBER 03 and GROMOS 53A6, to simulate the well-known Dickerson–Drew

\* To whom correspondence should be addressed: E-mail: netz@iq.ufrgs.br.

[ DADE ]				[ DAD3 ]				[ DAD5 ]			
[ atoms ]				[ atoms ]				[ atoms ]			
P	P	0.99000	0	P	P	0.99000	0	H5*	H	0.36000	0
O1P	OM	-0.63500	0	O1P	OM	-0.63500	0	O5*	OA	-0.36000	0
O2P	OM	-0.63500	0	O2P	OM	-0.63500	0	C5*	CH2	0.00000	1
O5*	OA	-0.36000	0	O5*	OA	-0.36000	0	C4*	CH1	0.16000	2
C5*	CH2	0.00000	1	C5*	CH2	0.00000	1	O4*	OA	-0.36000	2
C4*	CH1	0.16000	2	C4*	CH1	0.16000	2	C1*	CH1	0.20000	2
O4*	OA	-0.36000	2	O4*	OA	-0.36000	2	N9	NR	-0.20000	3
C1*	CH1	0.20000	2	C1*	CH1	0.20000	2	C4	C	0.20000	3
N9	NR	-0.20000	3	N9	NR	-0.20000	3	N3	NR	-0.54000	4
C4	C	0.20000	3	C4	C	0.20000	3	C2	C	0.44000	4
N3	NR	-0.54000	4	N3	NR	-0.54000	4	H2	HC	0.10000	4
C2	C	0.44000	4	C2	C	0.44000	4	N1	NR	-0.54000	5
H2	HC	0.10000	4	H2	HC	0.10000	4	C6	C	0.54000	5
N1	NR	-0.54000	5	N1	NR	-0.54000	5	N6	NT	-0.83000	6
C6	C	0.54000	5	C6	C	0.54000	5	H61	H	0.41500	6
N6	NT	-0.83000	6	N6	NT	-0.83000	6	H62	H	0.41500	6
H61	H	0.41500	6	H61	H	0.41500	6	C5	C	0.00000	7
H62	H	0.41500	6	H62	H	0.41500	6	N7	NR	-0.54000	7
C5	C	0.00000	7	C5	C	0.00000	7	C8	C	0.44000	7
N7	NR	-0.54000	7	N7	NR	-0.54000	7	H8	HC	0.10000	7
C8	C	0.44000	7	C8	C	0.44000	7	C2*	CH2R	0.00000	8
H8	HC	0.10000	7	H8	HC	0.10000	7	C3*	CH1	0.000	8
C2*	CH2R	0.00000	8	C2*	CH2R	0.00000	8	O3*	OA	-0.360	9
C3*	CH1	0.000	8	C3*	CH1	0.000	8	H3*	H	0.360	9
O3*	OA	-0.360	9								

**Figure 2.** Example of topology modification: from the original topology file (DADE), the 3' terminal nucleotide topology file (DAD3) was built by adding a hydrogen atom H3\* to the 3' extremity, whereas the 5' terminal nucleotide topology file (DAD5) was built by replacement of the atoms P, O1P, and O2P by an H5\* atom.

dodecamer. This dodecamer has the sequence d(CGCGAATTCGCG)<sub>2</sub> and its crystal structure (the first single-crystal structure of a DNA double helix) was elucidated in 1980.<sup>28–31</sup> This sequence is also known as the EcoRI dodecamer, since it contains the recognition site for the EcoRI restriction endonuclease.<sup>32</sup>

While there are several studies regarding DNA simulations with AMBER force fields,<sup>33–37</sup> the GROMOS force field has not yet received an extensive critical validation, with very few examples of relatively short DNA simulations ( $\leq 5$  ns).<sup>22,38–42</sup> Also, only the AMBER force field contains specific topologies for the terminal nucleotides (5' or 3'), while the GROMOS force field defines the terminal and nonterminal nucleotides in the same way. Thus, we decided to investigate the effect not only of the force field but also of the terminal nucleotide definitions upon the structure of the Dickerson–Drew dodecamer in simulations of 25 ns.

## Methods

We performed molecular dynamics simulations on the Dickerson–Drew dodecamer<sup>28–31</sup> d(CGCGAATTCGCG)<sub>2</sub>, comparing the AMBER 03<sup>18</sup> and GROMOS 53A6<sup>21</sup> force fields. The GROMOS 53A6 force field is based upon GROMOS 45A4, a force field that has undergone some refinement in order to better reproduce DNA crystallographic features.<sup>41</sup> Even so, the GROMOS 53A6 force field has topology parameters for nonterminal nucleotides only (DADE, DTHY, DCYT, and DGUA). In the AMBER force field, besides the usual nucleotide topology files (DA, DT, DC, and DG), there are specific topology files for 5' and 3' terminal nucleotides. In this way, considering the standard parametrization of each force field, the DNA structure simulated with GROMOS will exhibit two 5' terminal phosphate groups which would be absent if the DNA was simulated with AMBER.

In order to investigate not only the force field but also the effect of the terminal definitions, we performed simulations with each force field (GROMOS and AMBER), with and without consideration of the 5' terminal phosphates, consisting therefore of four systems, namely,

- system 1: AMBER 03 without terminal phosphates (AMBER standard topology)
- system 2: AMBER 03 with terminal phosphates (AMBER nonstandard topology)
- system 3: GROMOS 53A6 without terminal phosphates (GROMOS modified topology)
- system 4: GROMOS 53A6 with terminal phosphates (GROMOS standard topology)

The initial structure without the 5' terminal phosphates (systems 1 and 3) was taken from the AMBER force field port for GROMACS (<http://chemistry.csulb.edu/ffamber/>),<sup>43</sup> whereas the initial dodecamer structure with the terminal 5' phosphates (systems 2 and 4) was generated as a B-canonical conformation using the *fiber* module of the 3DNA package<sup>44</sup> with further modification of the atom and residue names, according to the force field. Apart from the terminal phosphate groups, there is a good overall structural agreement between both starting structures (rmsd = 0.111 989 nm).

According each force field construction, oligonucleotides bearing terminal 5' phosphates (systems 2 and 4) can be simulated with either force field. However, structures without terminal phosphates can only be directly simulated using AMBER, not with the original GROMOS. Therefore, eight new different topologies for terminal nucleotides were defined (DAD5, DAD3, DCY5, DCY3, DGU5, DGU3, DTH5, and DTH3) compatible with the GROMOS 53A6 force field. In order to construct these topology files, a hydrogen replaced the phosphate group (in the 5' terminal nucleotides) and a hydrogen was bonded to the terminal oxygen (in the 3' terminal nucleotides). In each case, the new atom must have a charge of +0.36, in order to build a neutral charge group. These modifications are shown in Figure 2 for the case of adenine only, since the other new topologies were built in a similar way.

All the simulations were carried out with the GROMACS package<sup>45–47</sup> either using the GROMOS 53A6 force field files (with the new topologies when needed) or using the AMBER 03 force field ports. The following generic simulation protocol was applied: box generation by placing the dodecamer in the center of a box with boundaries at least 1.8 nm apart from all

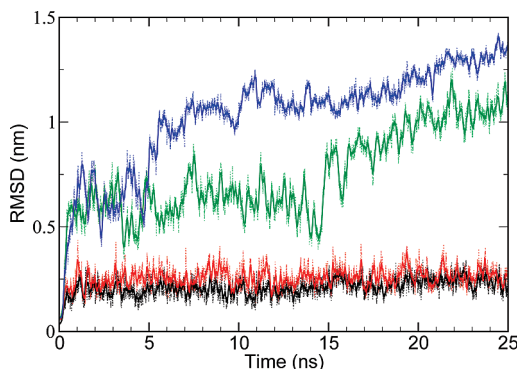


**Figure 3.** Atom positional root mean square deviation (rmsd), calculated along the MD trajectories for all atoms belonging to the Dickerson–Drew dodecamer, with respect to the original structures. Black line, system 1 (AMBER without terminal phosphates); red line, system 2 (AMBER with terminal phosphates); green line, system 3 (GROMOS without terminal phosphates); blue line, system 4 (GROMOS with terminal phosphates).

atoms of the molecule, random placement of counterions (sodium ions), position restrained molecular dynamics in the vacuum (allowing the counterions to migrate to the energetically most favorable positions), addition of water molecules (SPC<sup>48</sup> model for GROMOS or TIP3P<sup>49</sup> model for AMBER), energy minimization, addition of ions leading to physiological concentration ( $\text{NaCl } 0.154 \text{ mol L}^{-1}$ ), energy minimization, and 100 ps of position restrained molecular dynamics with full solvated system.

After these initial steps, a heating ramp was applied, consisting of short (50 ps) consecutive simulations at temperatures of 50, 100, 150, 200, 250, and 300 K. After that, a 200 ps simulation at 310 K was carried out during which the systems were checked for stability. The production simulation consisted of 25 ns at 310 K. The time step was 0.002 ps, and the electrostatic interactions were calculated using PME,<sup>50,51</sup> with a Coulomb cutoff radius of 1.2 nm. The Lennard-Jones interactions were calculated with a two-range switch interaction (cutoff radius of 0.9 and 1.1 nm). A Berendsen thermostat was applied,<sup>52</sup> with coupling time of 0.1 ps. Constraints were applied to all bonds, calculated with the LINCS<sup>53</sup> and SETTLE<sup>54</sup> algorithms.

The simulation trajectories were analyzed with standard GROMACS tools in order to calculate the time evolution of the root mean square deviation (rmsd) and the time evolution of the intramolecular hydrogen bonds. The hydrogen bonds were defined using a geometrical criterion<sup>55</sup> (donor–acceptor distance less than 0.35 nm and acceptor–donor-hydrogen angle less than 30°).

The nucleotide-specific parameters<sup>12,56–58</sup> were calculated along the simulation trajectories, from 5 ps spaced snapshots, using 3DNA tools (*find-pair* and *analyze*). The overall structural stability was monitored by calculating the total number of conserved base pairs and the number of noncanonical (non-Watson–Crick) base pairs along the simulation time. The local deformations of the double helix were deducted from main chain torsion angles, groove widths,<sup>59</sup> local base-pair-step parameters, and bending dihls.<sup>60</sup>

## Results and Discussion

**Global Stability.** We first analyzed the effect of the force field and terminal nucleotide definition in the overall stability of the oligonucleotide. According to Figure 3, the structures simulated with AMBER 03 force field were remarkably more

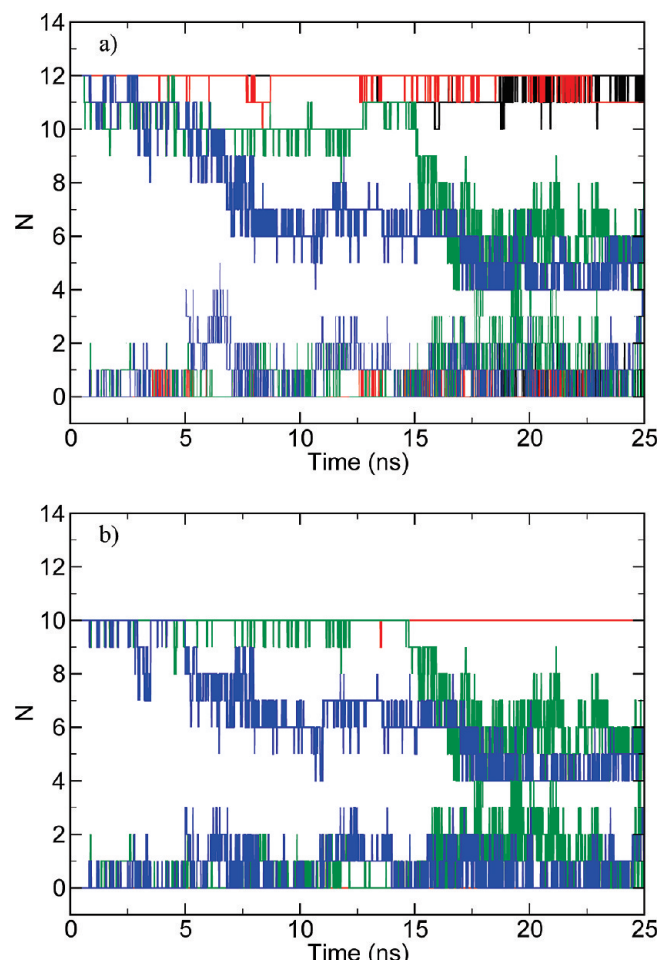


**Figure 4.** Number of conserved base pairs (upper curves) and number of non-Watson–Crick base pairs (bottom curves) for the studied systems, including the entire structure (a) or excluding the terminal base pairs (b). Black line, system 1 (AMBER without terminal phosphates); red line, system 2 (AMBER with terminal phosphates); green line, system 3 (GROMOS without terminal phosphates); blue line, system 4 (GROMOS with terminal phosphates).

stable than the structures simulated with GROMOS 53A6 force field. In both AMBER simulations (systems 1 and 2), the rmsd values averaged over the 0.2–0.3 nm interval, while the structures simulated with GROMOS (systems 3 and 4) reached extremely high rmsd values (>1.0 nm), also displaying very large fluctuations.

Although the definition of the terminal nucleotides did not affect the stability of DNA simulated with AMBER (systems 1 and 2), it clearly affected the stability of DNA when simulated with GROMOS (systems 3 and 4), resulting in lower values of rmsd when 5' terminal phosphate groups were suppressed (system 3).

Similar tendencies can be deduced from the analysis of the total number of canonical and noncanonical base pairs depicted in Figure 4a. In the systems simulated with AMBER force field, the 12 base pairs were conserved during almost the entire simulation, with a rather small number of non-Watson–Crick base pairs (between 0 and 2), as expected for this dodecamer.<sup>61</sup> Figure 4b, which excludes the terminal base pairs from the analysis, also shows that the eventual disruption of one or two base pairs seen in Figure 4a were restricted to the terminal regions in AMBER simulations.

On the other hand, the GROMOS simulations (systems 3 and 4) showed a much less stable profile, with progressive rupture

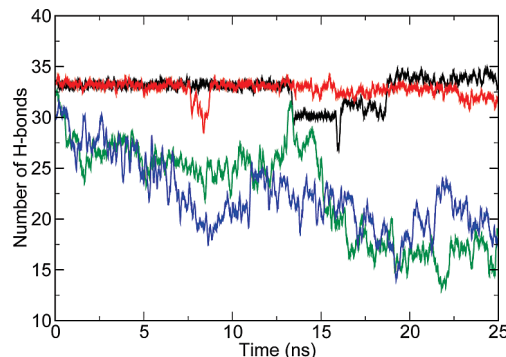


**Figure 5.** Number of intramolecular hydrogen bonds for the studied systems. Black line, system 1 (AMBER without terminal phosphates); red line, system 2 (AMBER with terminal phosphates); green line, system 3 (GROMOS without terminal phosphates); blue line, system 4 (GROMOS with terminal phosphates).

of the Watson–Crick base pairs and formation of several noncanonical base pairs (Figure 4a). Different from what was observed for AMBER, in GROMOS simulations the rupture of the base pairs was not restricted to the terminal region but rather propagated to the central region (Figure 4b), leading to an almost complete disruption of the double helix.

Nevertheless, again the proper definition of terminal nucleotides proved to have some positive effect in structural stability: GROMOS simulation with the 5' terminal phosphate (system 4) displayed a significant end-fraying effect in a very early stage (5 ns), probably associated with the repulsion between the charged phosphate groups, whereas the suppression of the charged terminal phosphate groups (system 3) shifted the denaturation to larger times (15 ns). Interestingly, the rmsd trajectories depicted in Figure 3 shows that DNA in system 4 endured an abrupt distortion at 5 ns, and that a similar pattern was observed for system 3 at 15 ns. Therefore, the end-fraying effect is very closely related to the large values of rmsd observed for DNA structures simulated with GROMOS. Also noteworthy is that, until now, the longest simulation performed with this dodecamer using GROMOS 53A6 consisted of 5 ns,<sup>22</sup> which appears to be a very critical time in DNA stability with GROMOS force field.

Finally, the pattern of the intramolecular hydrogen bonds (DNA–DNA) depicted in Figure 5 confirms that the structure of the oligonucleotides simulated with AMBER force field was well conserved, independently of the terminal nucleotide definition. In the simulations with the GROMOS force field, the number of hydrogen bonds decreased steadily and reached roughly half of the initial value. Altogether, these results are in agreement with a study performed by Arora and Jayaram,<sup>62</sup> who estimated the energetics of DNA base pairs via several potential energy functions (including AMBER and GROMOS) and predicted that base pair opening might be relatively facile with the GROMOS parameters.

**Backbone Parameters.** Although Calladine and Drew proposed that the DNA conformation is guided mainly by the  $\pi$ -stacking interactions between base pairs,<sup>63</sup> the backbone has also an important role since it restricts the available conformational space for stacking bases and couples the properties of the sequential neighboring nucleotides.<sup>64</sup> Therefore, we performed the analysis of some backbone torsional angles not only to access the conformational stability of the backbone during the simulations but also to correlate backbone alterations to base pairs movements and consequent helix deformations.

**$\alpha$  and  $\gamma$  Angles.** Among the backbone angles, the  $\alpha$  and  $\gamma$  angles are particularly important for the description of the low-

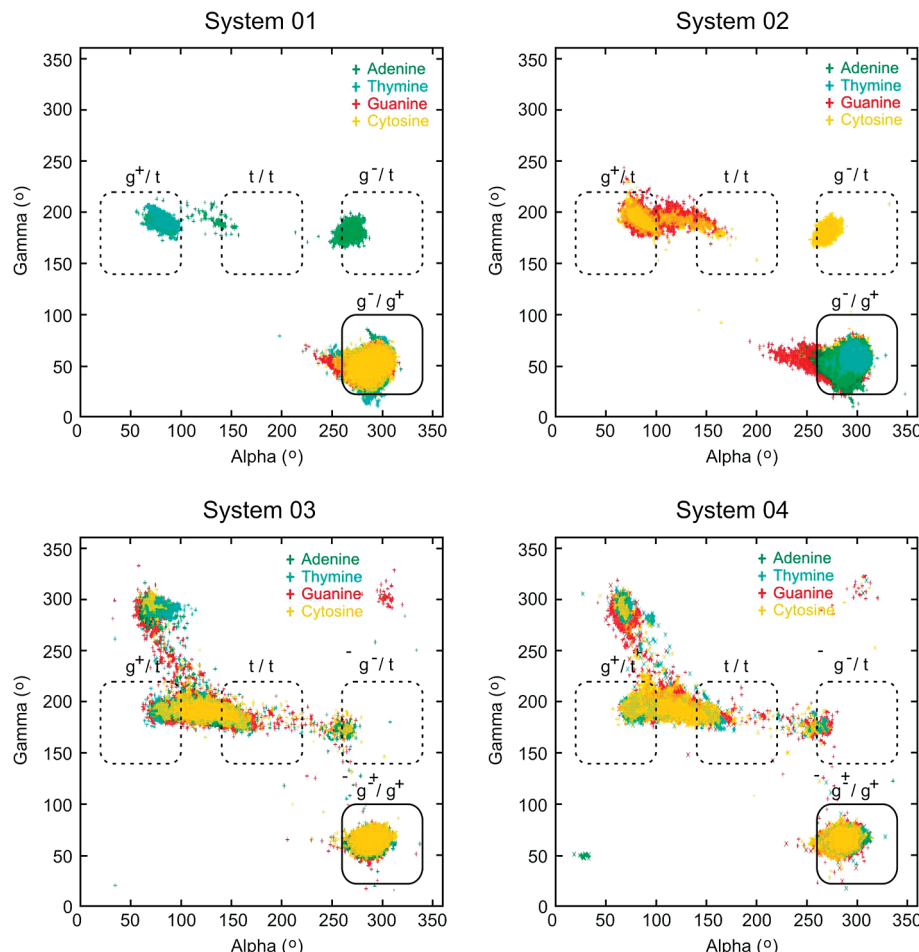
twist conformations that may be important during the recognition of DNA by proteins.<sup>65</sup> The AMBER force field is known to adequately sample canonical and noncanonical  $\alpha/\gamma$  conformations<sup>66</sup> and to display reversible transitions between the energetic minima, thus avoiding that the DNA remains stuck in a noncanonical conformation. However, besides the global minimum, with  $\alpha$  gauche minus and  $\gamma$  gauche ( $g^-/g^+$ ), the parm99 parametrization of the AMBER force field, upon which the AMBER 03 parametrization is based, is known to also favor a local minimum conformation ( $g^+/t$ ). This may lead to a field-dependent deformation of DNA in very large time scales (>20 ns), which was the motivation behind the recently proposed *parmBSC0* modification of the original AMBER parameters.<sup>66</sup> In the case of GROMOS 53A6, however, a complete description of the torsional sampling is still missing.

Figure 6 shows as scattered points the values of the  $\alpha$  and  $\gamma$  angles sampled in 5000 snapshots along the simulations for all nucleotides belonging to the first strand of the dodecamer. The results for the nucleotides belonging to the second strand (not shown) are very similar, with only slightly different nucleotide combinations but almost the same clustering pattern. The global minimum is defined in the area enclosed by the solid line and local minima are defined in the areas enclosed by dashed lines, according to Varnai et al.<sup>65</sup> These noncanonical  $\alpha/\gamma$  regions are essentially associated to altered values of roll and twist parameters, which describe curvature and winding of DNA double helix.<sup>65</sup>

In the AMBER simulations (systems 1 and 2), the most densely populated region corresponds to the  $g^-/g^+$  ground state, but both systems also allowed some restricted sampling of other local minima (mainly  $g^+/t$  and  $g^-/t$ ) (Figure 6). Although the AMBER systems presented similar  $\alpha/\gamma$  profiles, a small difference can be identified between them: system 2 appears to be subtly more dispersed than system 1, with a small population of the region  $t/t$  (associated with A-DNA<sup>67,68</sup>).

Concerning the GROMOS systems (3 and 4), Figure 6 shows a much more dispersed  $\alpha/\gamma$  profile, indicating that these simulations were less restricted to the canonical region when compared to those performed with AMBER. It is noteworthy that, because the DNA structure endured strong deformations in these simulations, 3DNA could not perform the analysis of the angles for all the 5000 snapshots. Actually, for system 3 the calculation of the backbone parameters could be performed in only 59% of the snapshots, whereas in system 4 only 18% of the configurations allowed this calculation. Therefore, considering that there is a smaller number of points in the graphics related to the GROMOS systems, one can conclude that the dispersion of the  $\alpha/\gamma$  angles was indeed dramatically increased. Besides an extensive sampling of two local minima ( $g^+/t$  and  $t/t$ ), there was a significant population of the region  $g^+/g^-$ , which is described as an energetically disfavored region of the  $\alpha/\gamma$  conformational landscape (5 kcal/mol<sup>69</sup>). Also, since there is a “path” of points between the regions  $g^+/t$  and  $t/t$ , there must be a very low energy barrier between these two states in the GROMOS force field, which allows the conformations to easily interconvert. This low energy barrier between  $g^+/t$  and  $t/t$  has been observed by Varnai et al.<sup>65</sup> for the parm99 force field, but our results showed it is even more negligible with the GROMOS force field, suggesting that GROMOS may facilitate transitions to the A-DNA isoform, which is known to assume the  $t/t$  conformation.<sup>67,68</sup>

The differences in the conformational landscape between the two force fields can be roughly estimated using the torsional energy profiles for the  $\alpha$  and  $\gamma$  angles, calculated with the force



**Figure 6.**  $\alpha/\gamma$  distribution. The values of  $\alpha$  and  $\gamma$  angles are shown as scatter plots for the four types of nucleotides in each simulated system. System 1, AMBER without terminal phosphates; system 2, AMBER with terminal phosphates; system 3, GROMOS without terminal phosphates; system 4, GROMOS with terminal phosphates. The global (solid line) and local (dashed line) minima are indicated.

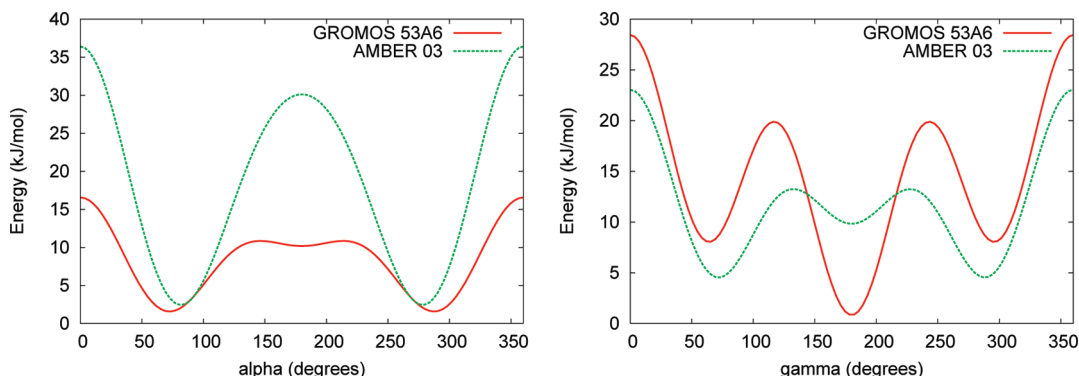


**Figure 7.** Pure torsional energy profiles for the backbone angles  $\alpha$  (left) and  $\gamma$  (right) calculated from the parameters of GROMOS and AMBER force fields.

field parameters, as shown in Figure 7. In this calculation, two aspects must be considered. First, the torsion angles in the GROMACS-ported version of AMBER (AMBERPORT) are described by Ryckaert–Bellemans functions,<sup>70,71</sup> that is, a series expansion in  $\cos(\phi)$ , whereas the GROMOS torsions keep the original functional form  $k_\phi(1 + \cos(n\phi - \phi_0))$ . Second, the GROMOS parametrization defines only one torsion for each central  $j-k$  bonded pair of atoms, which means that for each  $i-j-k-l$  only one pair  $i$  and  $l$  is given. The remaining torsions (other choices of  $i$  and  $l$ ) are coupled to the chosen one by the definition of improper dihedrals. The AMBER torsions, however, take explicitly into account all the torsions involving the

central bonded pair of atoms. In this way, the comparison between the effective torsional profiles must consider all the contributions in which the central bonded atoms participate.

Of course such estimate is only rough, because in the real systems the torsional terms are only one aspect that determine the actual value of the torsion angles, which also depend on the bonded and nonbonded interactions. Nevertheless, the torsional profiles shown in Figure 7 indeed explain some field-dependent differences in the  $\alpha/\gamma$  sampling. It shows that GROMOS clearly underestimates the  $\alpha$  barriers, also presenting a weak minimum at  $180^\circ$  that leads to the metastable  $\alpha:t$  conformation that was deduced from Figure 6. The GROMOS

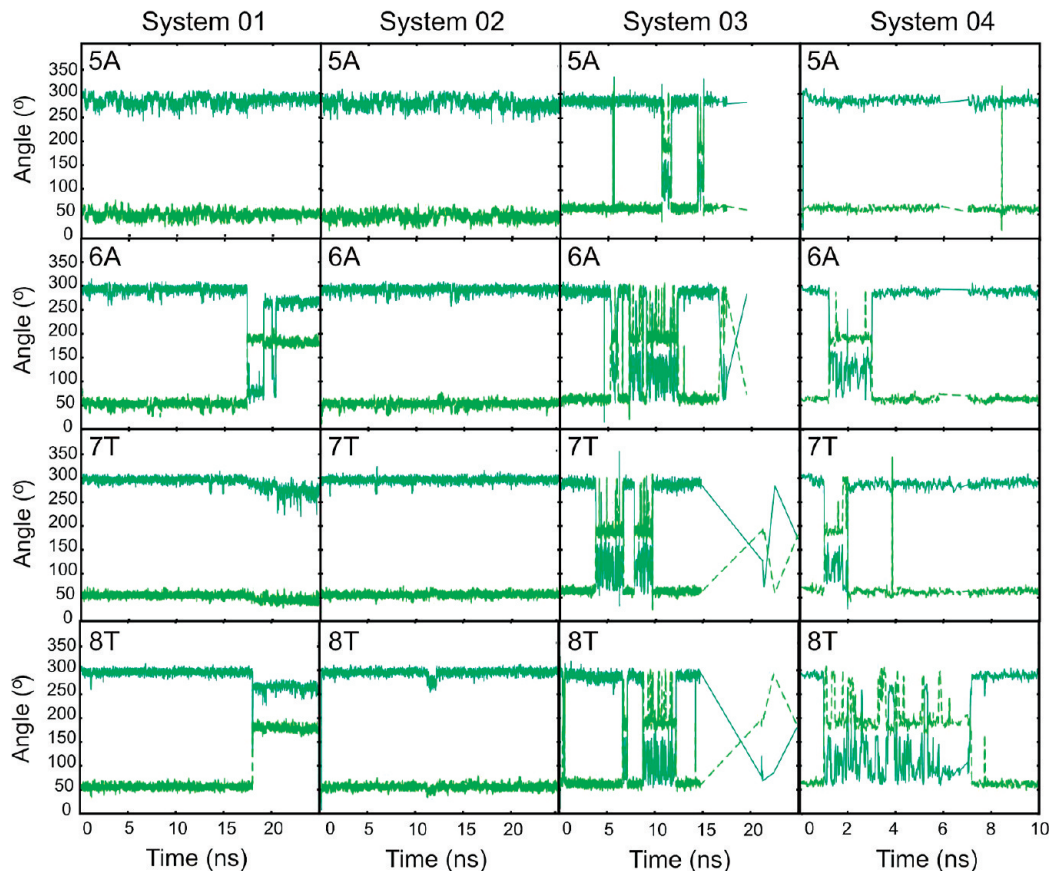


**Figure 8.** Temporal evolution of  $\alpha$  (dark green) and  $\gamma$  (light green) angles, for the strand I central region of the dodecamer in each simulated system. System 1, AMBER without terminal phosphates; system 2, AMBER with terminal phosphates; system 3, GROMOS without terminal phosphates; system 4, GROMOS with terminal phosphates.

force field also favors the  $\gamma:t$  conformation instead of the canonical  $\gamma:g^+$ , as can be deduced from the strong minimum at  $180^\circ$  in the  $\gamma$  profile.

Besides the quantification of the  $\alpha/\gamma$  conformations, it is also of major importance to analyze the frequency as well as the reversibility of these transitions, two aspects that can only be accessed by a temporal analysis as depicted in Figure 8. In this figure is shown the  $\alpha$  and  $\gamma$  evolution for the strand I central region (AATT) of the dodecamer in the four simulated systems. In the case of GROMOS simulation with terminal phosphate (system 4), the strong deformation of DNA prevented us to analyze the transitions beyond 10 ns.

We can observe in all systems a strong correlation between the  $\alpha$  and  $\gamma$  angles, which always endured concerted transitions. However, the two force fields significantly differed not only by the frequency but also by the time in which the transitions began to occur. In the AMBER force field (systems 1 and 2), there were few well-defined transitions, and the noncanonical conformations remained stable until the end of the simulations. The same analysis performed on other regions of this dodecamer (data not shown) proved that the DNA simulated with AMBER could return to the  $g^-/g^+$  conformation after remaining for several nanoseconds in noncanonical conformations. Moreover, none of the transitions in the central region occurred before the simulations reached 15 ns.

On the other hand, in the GROMOS simulations there were several fast and reversible transitions, some of them occurring very early in the simulations (before 2 ns in system 4). This extremely high frequency of transitions can be explained by the underestimation of the energy barriers separating the  $\alpha/\gamma$

states in the GROMOS force field, therefore leading to metastable substates instead of well-defined regions in the  $\alpha/\gamma$  conformational landscape.

Altogether, although changes in the terminal nucleotide definition lead to some small differences in the  $\alpha/\gamma$  transitions, the substantial differences were all due to the choice of the force field alone. The GROMOS force field showed an unbalanced, though reversible, sampling of noncanonical  $\alpha/\gamma$  conformations in the very beginning of the simulations and this may be the origin of the strong distortion observed for the DNA simulated with this force field. In this case, the flaw does not lie in the terminal phosphate definition and, as it was observed, the new parametrization used in system 3 cannot avoid the strong distortion of the DNA structure in the end of the simulation.

**$\varepsilon$  and  $\zeta$  Angles.** The  $\varepsilon$  and  $\zeta$  angles are strongly related to B-DNA flexibility, which is responsible for both target discrimination and structural adaptations upon DNA binding.<sup>8</sup> The combination of these two angles defines two subforms of B-DNA known as B-I (more frequent) and B-II (less frequent).<sup>67</sup> These conformers display two different phosphate geometries, with the phosphates in B-I being symmetrical in relation to the minor and major grooves, whereas in B-II the phosphates are deviated toward the minor groove.<sup>72</sup> The effect of B-II conformations upon the helicoidal parameters is not straightforward and depends on the symmetry of the B-II base pairs, being more pronounced when two B-II conformations are facing each other at the same dinucleotide step.<sup>8</sup>

According to Schneider et al.,<sup>67</sup> B-I conformation corresponds to  $\varepsilon:t/\zeta:g^-$  and B-II conformation corresponds to  $\varepsilon:g^-/\zeta:t$ . However, since these angles display large fluctuations, it can

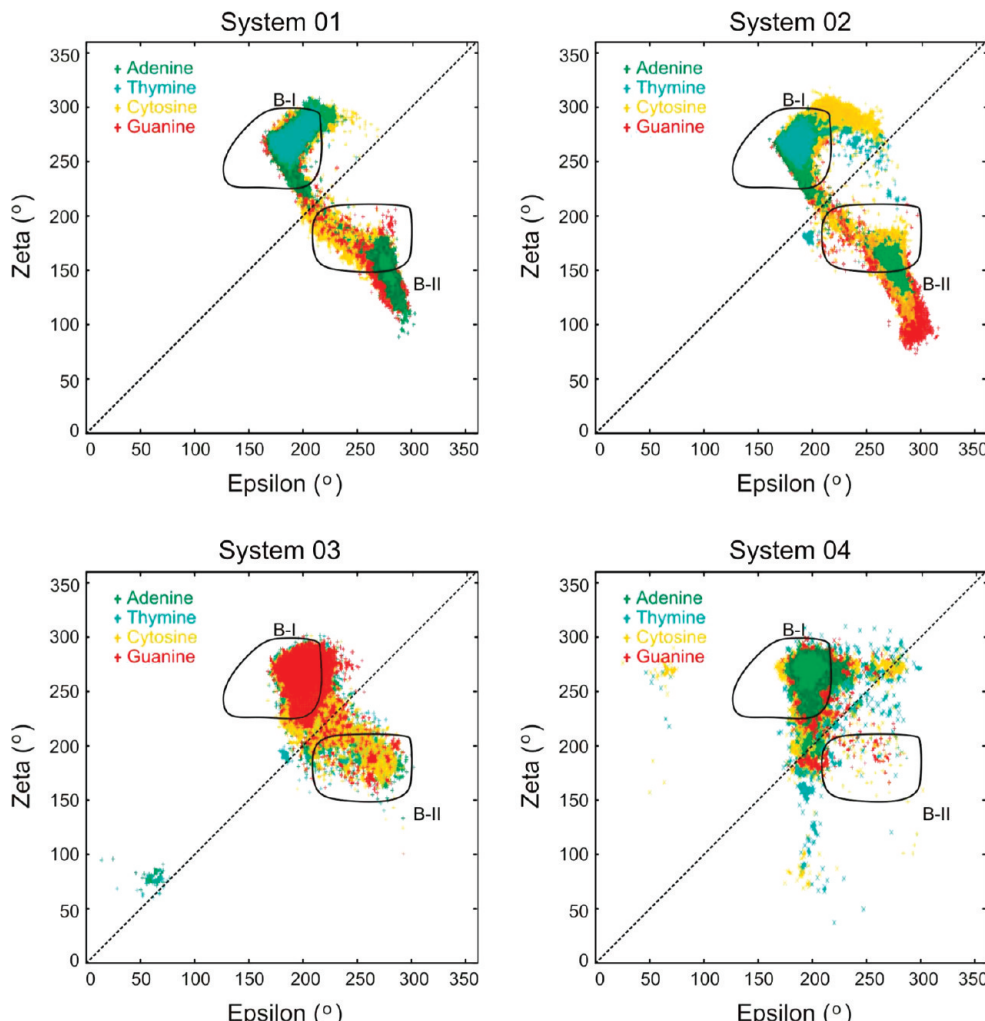


**Figure 9.**  $\varepsilon/\zeta$  angles distribution. The values of  $\varepsilon$  and  $\zeta$  angles are shown as scatter plots for the four types of nucleotides in each simulated system. System 1, AMBER without terminal phosphates; system 2, AMBER with terminal phosphates; system 3, GROMOS without terminal phosphates; system 4, GROMOS with terminal phosphates. The regions for the canonical conformations B-I and B-II are indicated.

be considered that a conformation belongs to the B-I form when the value of  $\varepsilon - \zeta \approx -90^\circ$ , whereas it belongs to the B-II conformation when  $\varepsilon - \zeta > 0^\circ$ . Figure 9 shows the  $\varepsilon$  and  $\zeta$  angles for all nucleotides along 5000 snapshots of the simulations, and the refined B-I and B-II regions are enclosed by dashed lines, according to Schneider et al.<sup>67</sup> The diagonal line can also be used as a coarse separation of B-I ( $\varepsilon - \zeta < 0^\circ$ ) and B-II ( $\varepsilon - \zeta > 0^\circ$ ) regions.

We can observe in Figure 9 that, as occurred with  $\alpha/\gamma$  angles, the systems simulated with AMBER force field (1 and 2) presented similar  $\varepsilon/\zeta$  profiles, proving to be robust to the change in the terminal nucleotide conditions. In both systems, the conformations were close clustered around the expected B-I and B-II regions, although in system 2 (with terminal phosphates) there was a small dispersion in a region close to B-I, which was not observed in system 1. Also, there is a recognizable “path” of points connecting the regions B-I and B-II. This suggests the existence of a metastable region involving concerted changes in  $\varepsilon$  and  $\zeta$  angles which is probably the lower energy path between the two minima.

Analyzing the same results for the GROMOS force field with terminal phosphate (Figure 9, system 4), we observe a much more dispersed  $\varepsilon/\zeta$  distribution (especially because, as already noted for the  $\alpha/\gamma$  angles, this plot presents a smaller number of points). Although the system 4 remained mainly in the B-I conformation, we do not observe a recognizable “path” con-

nnecting the regions B-I and B-II. Instead, it is very clear that most of the  $\varepsilon/\zeta$  transitions occurred in a nonconcerted fashion, in which only one of the angles was significantly changed per transition, leading to other regions that do not comprise B-I  $\rightarrow$  B-II transitions.

Remarkably, the deletion of the end phosphates and reparametrization of the terminal nucleotides in the system 3 caused a dramatic effect in the distribution of the  $\varepsilon/\zeta$  angles: not only did the points become more close clustered around B-I and B-II conformations but also a recognizable path of interconversion arose (Figure 9, system 3). Roughly, one could conclude that the deletion of the terminal phosphate funneled all the noncanonical conformations found in the system 4 into B-II conformations in the system 3. Moreover, GROMOS simulation without terminal phosphates (system 3) showed a remarkably small extent of B-II sampling when compared to the AMBER simulations, proving to be more conservative regarding DNA flexibility.

The time-resolved analysis of the B-I  $\rightarrow$  B-II transitions is shown in Figure 10. Since DNA endured a strong deformation in system 4, the analysis for this system was performed only for the first 5 ns. The comparison of the four simulated systems shows that, whereas the transitions in the AMBER systems depended on the sequence, the transitions for GROMOS simulation were nearly sequence-independent. In both force fields, the departures from B-I canonical conformation proved

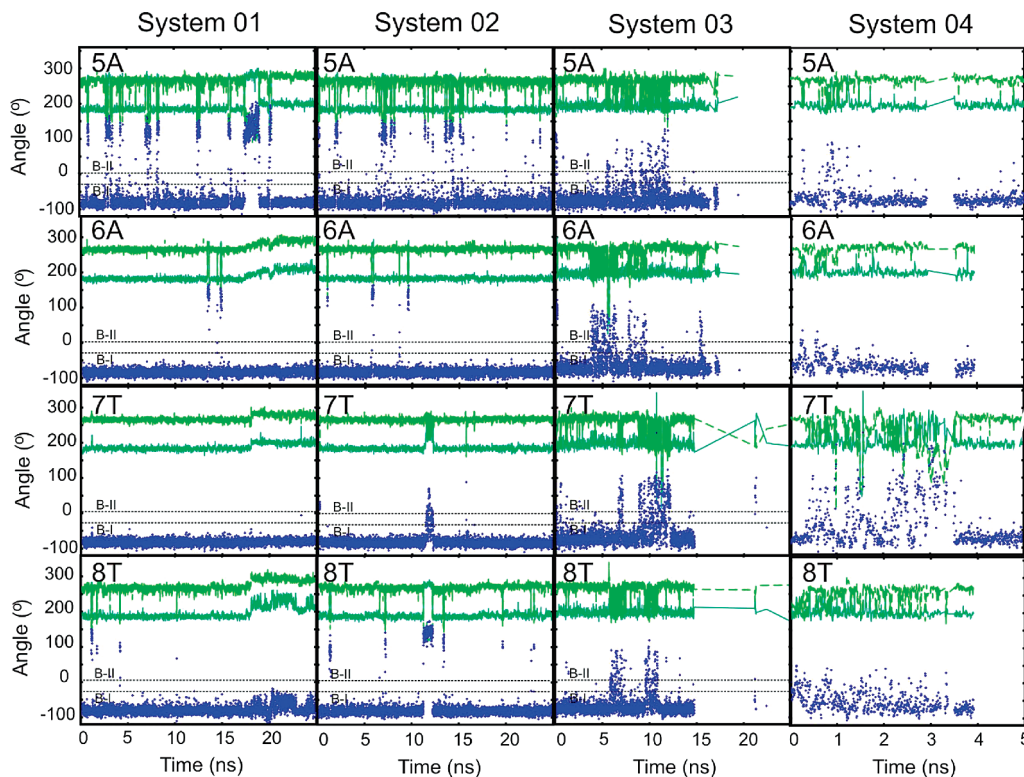


**Figure 10.** Temporal evolution of  $\epsilon$  (dark green) and  $\zeta$  (light green) angles, for the strand I central region of the dodecamer in each simulated system. The difference ( $\epsilon - \zeta$ ) is shown as blue points. System 1, AMBER without terminal phosphates; system 2, AMBER with terminal phosphates; system 3, GROMOS without terminal phosphates; system 4, GROMOS with terminal phosphates.

to be reversible. Although the B-II conformations were observed in the GROMOS simulations, they were not so frequently sampled, nor so well-defined as in the AMBER simulations. Unfortunately, it is not possible to observe a clear distinction between the temporal evolution of  $\epsilon/\zeta$  in systems 3 and 4 due to the very short analysis performed for system 4.

In short, it not only seems that the  $\epsilon/\zeta$  profile depends upon the choice of the force field but also that it is strongly affected by the terminal nucleotide definitions. Somehow, the deletion of terminal phosphates and reparametrization of the terminal nucleotides influenced the distribution of conformation over the  $\epsilon/\zeta$  conformational landscape. Since this new parametrization did not affect the torsional parameters, it is likely that, in this case, the torsional landscape was changed due to the nonbonded interactions (mainly electrostatic). Despite the fact that GROMOS simulation with terminal phosphate (system 4) resulted in a more dispersed  $\epsilon/\zeta$  profile, still the B-I was the most densely populated region. This suggest that  $\epsilon$  and  $\zeta$  angles are not as decisive during the denaturation process in GROMOS simulations as  $\alpha$  and  $\gamma$ . Nevertheless, the better reproduction of B-I  $\rightarrow$  B-II transitions acquired from the deletion of phosphates (system 3) may have provided some alternative stabilization for the distortions caused by the  $\alpha/\gamma$  transitions, therefore delaying, but not at all avoiding the denaturation process.

**Groove Widths.** The B-canonical conformation of DNA is known to display a pronounced asymmetry regarding the groove widths, but the actual value of these quantities is sequence-dependent and plays a major role during protein and ligand recognition. Sequences rich in adenine and thymine, as the central region of Dickerson dodecamer, are known for presenting extremely narrow minor grooves, which facilitates the binding of small minor groove ligands like netropsin.<sup>9,73</sup> Moreover, these widths can fluctuate during the simulations and the average value also depends upon the choice of the force field. The AMBER

family of force fields, for instance, is known for slightly overestimating the grooves asymmetry, enhancing the difference between the minor and the major groove widths.<sup>36</sup>

Figures 11 and 12 show the major and the minor groove widths, for the central region of the nucleotide, according to the definitions of El Hassan and Calladine.<sup>59</sup>

In the AMBER simulations, the terminal nucleotide definition did not play any role in the major or minor groove widths: the major groove displayed some fluctuation between 1.5 and 2.5 nm (Figure 11), whereas the minor groove remained remarkably stable around 1.2 nm (Figure 12). These values lead to a difference of approximately 0.6 nm between the two grooves, which is in agreement with the simulations performed by Perez et al.<sup>36</sup>

As a general trend, the major groove widths in the GROMOS simulations were somewhat larger, especially in the last 5 ns of the simulations, when they reached extremely high values (Figure 11). However, since the DNA is completely denatured at the end of the simulations, it is more interesting to analyze the groove widths in the first 5 ns (system 4) or 15 ns (system 3), before the denaturation propagated to the central region. Using this approach, a larger major groove is observed in both systems 3 and 4 (2–3 nm) when compared with systems 1 and 2.

Concerning the minor groove widths, the GROMOS systems also lead to larger minor grooves (>1.2 nm) in comparison to the AMBER simulations (Figure 12). Moreover, it was clearly observed that system 3 (without terminal phosphates) produced a much more stable profile than system 4 (with terminal phosphates) regarding the minor groove geometry.

In general, we can think of three main ways of affecting the groove widths: (i) through B-I  $\rightarrow$  B-II transitions (which enhances the major groove over the minor groove);<sup>72</sup> (ii) through bending (bending toward the minor groove enhances the major

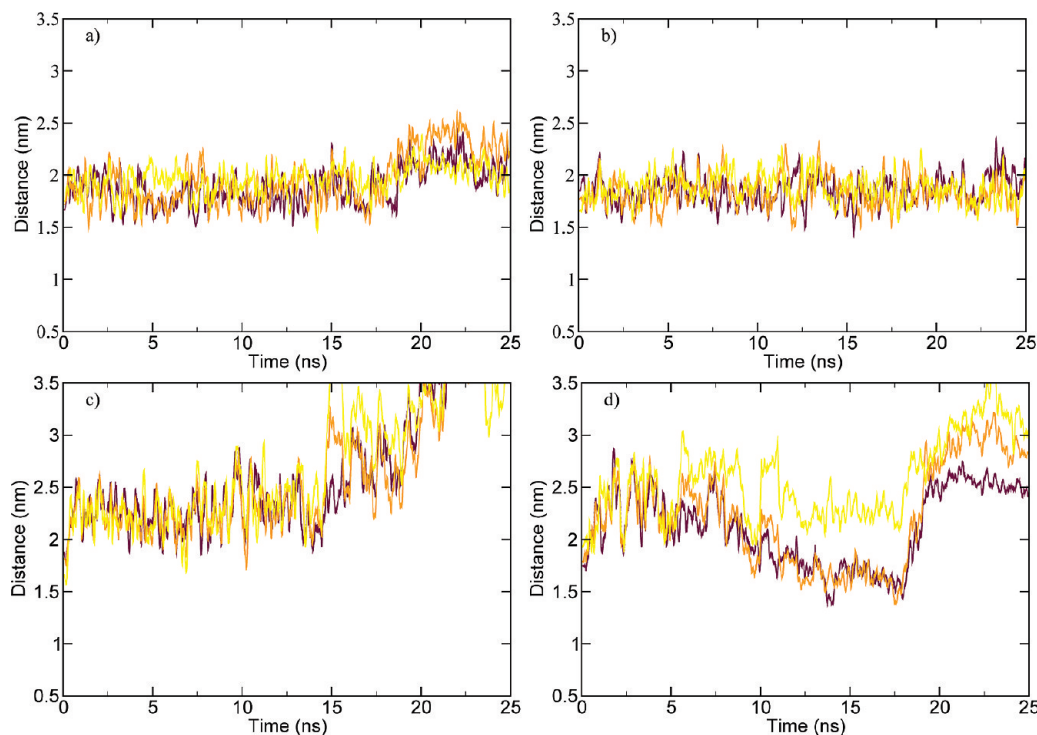


**Figure 11.** Central portion major groove widths, as measured according to El Hassan and Caladine:<sup>59</sup> brown lines, P4–P17; orange lines, P5–P16; yellow lines, P6–P15. (a) system 1, AMBER without terminal phosphates; (b) system 2, AMBER with terminal phosphates; (c) system 3, GROMOS without terminal phosphates; (d) system 4, GROMOS with terminal phosphates.

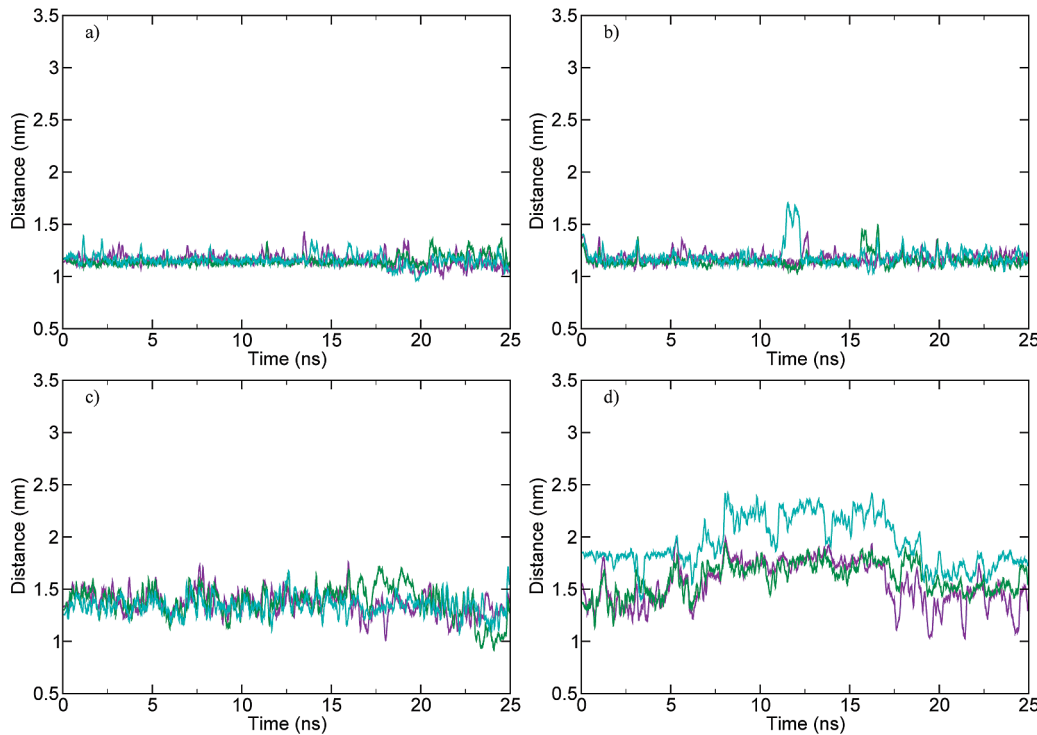


**Figure 12.** Central portion minor groove widths, as measured by the distance between phosphates. Violet lines: P7–P21; green lines: P8–P20; cyan lines: P9–P19. (a) system 1, AMBER without terminal phosphates; (b) system 2, AMBER with terminal phosphates; (c) system 3, GROMOS without terminal phosphates; (d) system 4, GROMOS with terminal phosphates.

groove and vice versa<sup>5</sup>); and (iii) by changing the torsion angle (a decrease in the twist enhances both major and minor groove). Among these, only a decrease in twist would allow for a concerted increase of both grooves, as was observed for GROMOS when compared with AMBER. Therefore, it is very likely that the DNA simulated with GROMOS will also present

lower values of twist when compared to AMBER simulations, an aspect that will be discussed in the following section.

The minor groove width apparently seems to be less affected by the denaturation as the major groove width, as seen for the system 3 (comparing Figure 12c and Figure 11c). Visual inspection of the trajectory has shown that indeed the denatur-

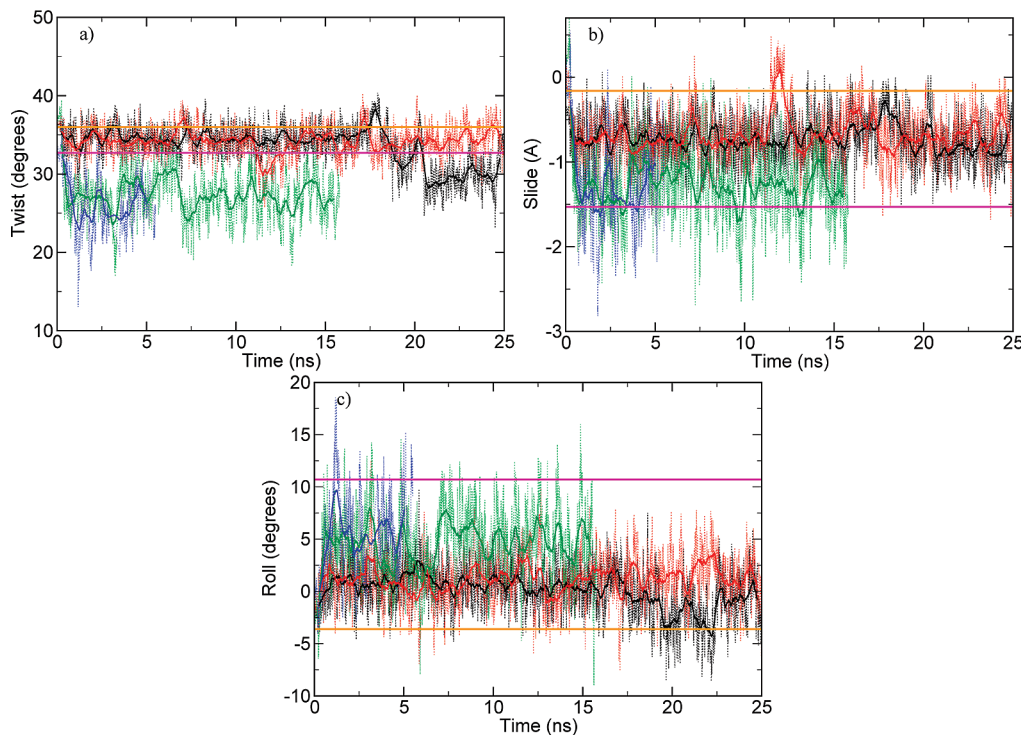


**Figure 13.** Average twist (a), slide (b), and roll (c) for the central (AATT) portion of the dodecamer. Black line, system 1 (AMBER without terminal phosphates); red line, system 2 (AMBER with terminal phosphates); green line, system 3 (GROMOS without terminal phosphates); blue line, system 4 (GROMOS with terminal phosphates). The sequence-averaged experimental results for A-DNA and B-DNA (from ref 33) are shown in magenta and orange, respectively.

ation process in the systems 3 and 4 occurs early and it is more pronounced in the major groove than in the minor groove. Even when the structure was significantly denatured, the central portion of the dodecamer showed a more or less conserved minor groove. Besides that, according to the chosen definition for the grooves' width calculation,<sup>59</sup> the metrics for the major groove width correlates with regions more distant from the central part and is more sensitive to structure changes that start from the ending base pairs, as usual in the DNA denaturation.

**Base-Pair Step Parameters.** Among the several base-pair parameters that can be used to describe DNA structure, we chose twist, slide, and roll (Figure 13) to perform the analysis. According to El Hassan and Calladine,<sup>74</sup> the conformational space of any dinucleotide step is almost completely defined by these three base step parameters. Moreover, these authors have shown a general positive correlation between twist and slide, and a negative correlation between slide/twist and roll, which are probably mechanical consequences of the conformational boundaries imposed by the backbone.<sup>74</sup>

According to Figure 13, the results of twist, slide, and roll in the AMBER simulations were reasonably close to the crystallographic B-DNA average values.<sup>33</sup> As already noted for the AMBER family of force fields, it produced twist angles 3–4° lower in average than the crystallographic angles,<sup>75</sup> which is accompanied by slightly lower and higher values of slide and roll, respectively.

The same analysis performed for GROMOS shows that systems 3 and 4 produced values of base-pair parameters which are far more distant from experimental B-DNA results (Figure 13), also displaying large fluctuations after 5 ns (system 4) and 15 ns (system 3) (data not shown). These very large fluctuations are most likely artifactual since their beginning correlates very well with the severe denaturation endured by DNA in these systems (see the subsection Global Stability). For that reason, we only presented the results for the simulation stages previous

to denaturation. It is observed that, on average, GROMOS strongly underestimated twist ( $27 \pm 3^\circ$ ) and slide ( $-1.3 \pm 0.4 \text{ \AA}$ ) and overestimated roll ( $4 \pm 3^\circ$ ) in both systems 3 and 4. Therefore, even before the denaturation takes place, the GROMOS force field lead to an unwound double helix which is distant from the canonical B-DNA, but coarsely resembles the A-form of DNA, which also displays low twist ( $32^\circ$ ), negative slide ( $-1.5 \text{ \AA}$ ), and positive roll ( $12^\circ$ ).<sup>33</sup>

Indeed, this low twist profile for GROMOS simulations was expected and can be correlated with two other results previously presented in this work: (i) the high population of  $\alpha/\gamma$  noncanonical conformations observed in GROMOS simulations, especially the trans/trans region (see the subsection Backbone Parameters); (ii) the concerted widening of both minor and major grooves in DNA simulated with GROMOS, which could only be achieved by unwinding of the double helix (see the section about Groove Widths).

The local bending was characterized using the bending dials (Figure 14),<sup>60</sup> which corresponds to a vectorial combination of roll and tilt parameters yielding a deflection  $\theta$  parameter and an orientation  $\phi$  parameter, displayed in polar coordinates. The bending dials allow a precise characterization of the local curvature: distribution in the northern hemisphere corresponds to local bending toward the major groove (MG) while distribution in the southern hemisphere corresponds to local bending toward the minor groove (mg). The distribution of the points in the east or west corresponds to local bending toward one of the phosphate backbone strands. In the figure, each ring corresponds to a  $5^\circ$  deflection of the helical axis.

In the AMBER systems, an east–west symmetry was observed, which was expected since the Dickerson sequence is palindromic, and a slight displacement of the population over the north hemisphere was observed, which was also expected since TA/TA steps are known for presenting high values of roll that lead to major groove bending.<sup>74,76</sup> In the GROMOS systems,

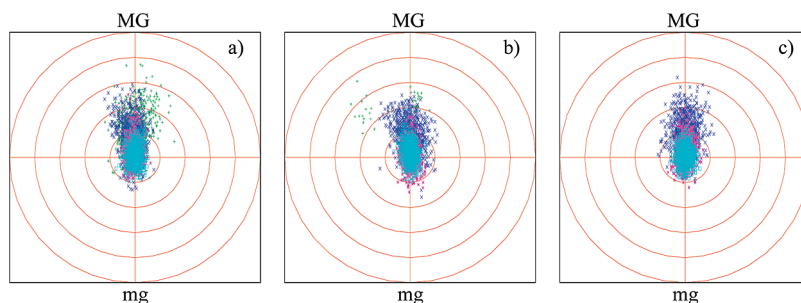


**Figure 14.** Average magnitude and directionality of the curvature of the central (AATT) region of the dodecamer as measured by the bending dials. Shown as scattered points are the results for system 1 (light blue), system 2 (magenta), system 3 (dark blue), and system 4 (green). The three plots correspond to the time intervals 0–5 ns (a), 5–10 ns (b), and 10–15 ns (c). Each ring corresponds to a 5° deflection of the helical axis (the largest is 25°).

a more pronounced population of the north region was observed, but it is not clear whether this indicates a change in the direction of the double helix (global curvature) or a change in the helix conformation ( $B \rightarrow A$  transition).

## Conclusions

We performed 25 ns simulations with the Dickerson dodecamer, using two different force fields, AMBER 03 and GROMOS 53A6. Since the AMBER force field possesses special topologies for the terminal nucleotides while the GROMOS force field does not, we also investigated the effect of terminal nucleotide definition upon each force field. In this way, we also simulated the dodecamer with a simplified version of AMBER (without terminal nucleotide topologies) and with a modified version of GROMOS (with terminal nucleotide topologies).

The choice of force field and, in the case of GROMOS, the terminal nucleotide definition, proved to have a pronounced effect on the structure and stability of DNA double helix. Simulations with AMBER force field were very stable and reproduced the experimental parameters for the Dickerson–Drew dodecamer independently of the terminal nucleotide definitions. On the other hand, analysis of rmsd, number of base pairs, and base-pair steps all indicate that the DNA simulated with the original GROMOS 53A6 endured strong distortions after 5 ns (system 4) but this effect was delayed to 15 ns when terminal nucleotide topologies were applied (system 3). Hitherto, this field-dependent instability was never shown in such a peremptory way, probably because the longest DNA simulation using GROMOS consisted of 5 ns, which seems to be a very crucial time regarding DNA stability with the GROMOS force field.

While the global distortions of DNA in GROMOS systems became more evident only after 5 ns, several transitions to noncanonical  $\alpha/\gamma$  conformations occurred very early in the simulations and are probably the origin of DNA deformation. Among the noncanonical  $\alpha/\gamma$  conformations, there was an extensive sampling of the  $\alpha(\text{trans})/\gamma(\text{trans})$  region characteristic of A-DNA, which is very likely the origin of the low twist DNA conformations observed in the GROMOS simulations. Undoubtedly, the very low torsional barriers between global and local minima in the  $\alpha/\gamma$  conformational landscape are one of the major flaws of the GROMOS force field concerning nucleic acids simulations.

While the  $\alpha/\gamma$  distribution was affected by the choice of the force field only, the  $\varepsilon/\zeta$  angles in the GROMOS force field were affected by both the force field and the terminal nucleotide definition. Remarkably, the deletion of terminal phosphate groups in the GROMOS new parametrization affected the distribution on the  $\varepsilon/\zeta$  conformational landscape, providing a defined energy path for  $B\text{-I} \rightarrow B\text{-II}$  transitions that was not

observed for the original GROMOS parametrization. Since these transitions can also occur very early in the simulations, it might be possible that the acquired flexibility toward the B-II conformation somehow stabilizes the noncanonical  $\alpha/\gamma$  conformations, therefore delaying, but not avoiding the disruption of the double helix in GROMOS simulations.

In conclusion, despite being a very successful force field for simulating proteins, GROMOS 53A6 leads to strong distortion of DNA, culminating in the complete disruption of the double helix after 5 ns. The definition of terminal nucleotide topologies presented in this work proved to be a step toward the improvement of this force field; however, a further reparametrization is still needed especially regarding the torsional parameters.

**Acknowledgment.** We acknowledge the financial support from Coordenação de Aperfeiçoamento de Pessoal de Nível Superior (CAPES) and Conselho Nacional de Desenvolvimento Científico e Tecnológico (CNPq) 474810/2008-9 Edital Universal.

## References and Notes

- Norberg, J.; Nilsson, L. *Q. Rev. Biophys.* **2003**, *36*, 257–306.
- Moraitakis, G.; Purkiss, A. G.; Goodfellow, J. M. *Rep. Prog. Phys.* **2003**, *66*, 383–406.
- Mackerell, A. D., Jr. *J. Comput. Chem.* **2004**, *25*, 1584–1604.
- Giudice, E.; Lavery, R. *Acc. Chem. Res.* **2002**, *35*, 350–357.
- Travers, A. A. *Philos. Trans. R. Soc. London* **2009**, *362*, 1423–1438.
- Lavery, R. *Nucleic Acids Res.* **2010**, *38*, 299–313.
- Dickerson, R. E.; Chiu, T. K. *Biopolymers* **1998**, *44*, 361–403.
- Djurjanovic, D.; Hartmann, B. *Biopolymers* **2004**, *73*, 356–368.
- Neidle, S. *Biopolymers* **1997**, *44*, 105–121.
- Ahmad, S.; Kono, H.; Arauzo-Bravo, M. J.; Sarai, A. *Nucleic Acids Res.* **2006**, *34*, W124–W127.
- Hurley, L. H. *Nature Rev. Cancer* **2002**, *2*, 188–200.
- Dickerson, R. E.; Drew, H. R.; Conner, B. N.; Wing, R. M.; Fratini, A. V.; Kopka, M. L. *Science* **1982**, *216*, 475–485.
- Mackerell, A. D., Jr.; Kuczera, J. W.; Karplus, M. *J. Am. Chem. Soc.* **1995**, *117*, 11946–11975.
- Mackerell, A. D., Jr.; Banavali, N. *J. Comput. Chem.* **2000**, *21*, 105–120.
- Foloppe, N.; Mackerell, A. D., Jr. *J. Comput. Chem.* **2000**, *21*, 86–104.
- Cornell, W. D.; Cieplak, P.; Bayly, C. I.; Gould, I. R.; Merz, K. M., Jr.; Ferguson, D. M.; Spellmeyer, D. C.; Fox, T.; Caldwell, J. W.; Kollman, P. A. *J. Am. Chem. Soc.* **1995**, *117*, 5179.
- Wang, J.; Cieplak, P.; Kollman, P. A. *J. Comput. Chem.* **2000**, *21*, 1049–1074.
- Duan, Y.; Wu, C.; Chowdhury, S.; Lee, M. C.; Xiong, G.; Zhang, W.; Yang, R.; Cieplak, P.; Luo, R.; Lee, T.; Caldwell, J.; Wang, J.; Kollman, P. *J. Comput. Chem.* **2003**, *24*, 1999–2012.
- van Gunsteren, W. F.; Billeter, S. R.; Eising, A. A.; Hunenberger, P. H.; Kruger, P.; Mark, A. E.; Scott, W. R. P.; Tironi, I. G. In *Biomolecular simulation: The GROMOS96 Manual and User guide*; Vdf Hochschulverlag AG: Zurich, Switzerland; pp 1–1042.

- (20) Scott, W. R. P.; Hunenberger, P. H.; Tironi, I. G.; Mark, A. E.; Billeter, S. R.; Fennen, J.; Torda, A. E.; Huber, T.; Kruger, P.; van Gunsteren, W. F. *J. Phys. Chem. A* **1999**, *103*, 3596–3607.
- (21) Oostenbrink, C.; Villa, A.; Mark, A. E.; van Gunsteren, W. F. *J. Comput. Chem.* **2004**, *25*, 1656–1676.
- (22) Oostenbrink, C.; Soares, T. A.; van der Vegt, N. F. A.; van Gunsteren, W. F. *Eur. Biophys. J.* **2005**, *34*, 273–284.
- (23) Jorgensen, W. L.; Tirado-Rives, J. *J. Am. Chem. Soc.* **1988**, *110*, 1657–1666.
- (24) Jorgensen, W. L.; Maxwell, D. S.; Tirado-Rives, J. *J. Am. Chem. Soc.* **1996**, *118*, 11225–11236.
- (25) Levitt, M.; Hirshberg, M.; Sharon, R.; Daggett, V. *Comput. Phys. Commun.* **1995**, *91*, 215–231.
- (26) Langley, D. R. *J. Biomol. Struct. Dyn.* **1998**, *16*, 487–509.
- (27) Feig, M.; Pettitt, B. M. *Biophys. J.* **1998**, *75*, 134–139.
- (28) Wing, R. M.; Drew, H. R.; Takano, T.; Broka, C.; Tanaka, S.; Itakura, I.; Dickerson, R. E. *Nature* **1980**, *287*, 755–758.
- (29) Dickerson, R. E.; Drew, H. R. *J. Mol. Biol.* **1981**, *149*, 761–786.
- (30) Drew, H. R.; Wing, R. M.; Takano, T.; Broka, C.; Tanaka, S.; Itakura, K.; Dickerson, R. E. *Proc. Natl. Acad. Sci. U.S.A.* **1981**, *78*, 2179–2183.
- (31) Drew, H. R.; Dickerson, R. E. *J. Mol. Biol.* **1981**, *151*, 535–556.
- (32) Beveridge, D. L.; McConnell, K. J. *Curr. Opin. Struct. Biol.* **2000**, *10*, 182–196.
- (33) Reddy, S. Y.; Leclerc, F.; Karplus, M. *Biophys. J.* **2003**, *84*, 1421–1449.
- (34) Babin, V.; Baucom, J.; Darden, T. A.; Sagui, C. *J. Phys. Chem. B* **2006**, *110*, 11571–11581.
- (35) Perez, A.; Luque, F. J.; Orozco, M. *J. Am. Chem. Soc.* **2007**, *129*, 14739–14745.
- (36) Perez, A.; Lankas, F.; Luque, F. J.; Orozco, M. *Nucleic Acids Res.* **2008**, *36*, 2379–2384.
- (37) Mura, C.; McCammon, J. A. *Nucleic Acids Res.* **2008**, *36*, 4941–4955.
- (38) Tapia, O.; Velasquez, I. *J. Am. Chem. Soc.* **1997**, *119*, 5934–5938.
- (39) Bonvin, A. M. J. J.; Sunnerhagen, M.; Otting, G.; van Gunsteren, W. F. *J. Mol. Biol.* **1998**, *282*, 859–873.
- (40) Swaminathan, S.; Ravishanker, G.; Beveridge, D. L. *J. Am. Chem. Soc.* **1991**, *113*, 5027–5040.
- (41) Soares, T. A.; Hunenberger, P. H.; Kastenholtz, M. A.; Krautler, V.; Lenz, T.; Lins, R. D.; Oostenbrink, C.; van Gunsteren, W. F. *J. Comput. Chem.* **2005**, *26*, 725–737.
- (42) Bonvin, A. M. J. J. *Eur. Biophys. J.* **2000**, *29*, 57–60.
- (43) Sorin, E. J.; Pandé, V. S. *Biophys. J.* **2005**, *88*, 2472–2493.
- (44) Lu, X. J.; Olson, W. K. *Nucleic Acids Res.* **2003**, *31*, 5108–5121.
- (45) Lindahl, E.; Hess, B.; van der Spoel, D. *J. Mol. Modell.* **2001**, *7*, 306–317.
- (46) van der Spoel, D.; Lindahl, E.; Hess, B.; van Buuren, A. R.; Apol, E.; Meulenhoff, P. J.; Tielman, D. P.; Sijbers, A. L. T. M.; Feenstra, K. A.; van Drunen, R.; Berendsen, H. J. C. Gromacs User Manual version 3.3; www.gromacs.org, 2005.
- (47) van der Spoel, D.; Lindahl, E.; Hess, B.; Groenhof, G.; Mark, A. E.; Berendsen, H. J. C. *J. Comput. Chem.* **2005**, *26*, 1701–1718.
- (48) Berendsen, H.; Postma, J.; Gunsteren, W.; Hermans, J. In *Interaction Models for Water in Relation to Protein Hydration*; Pullman, B., Ed.; D. Reidel Publishing Co.: Amsterdam, 1981; p 331.
- (49) Jorgensen, W. L.; Chandrasekhar, J.; Madura, J. D.; Impey, R. W.; Klein, M. L. *J. Chem. Phys.* **1983**, *79*, 926–935.
- (50) Darden, T.; York, D.; Pedersen, L. G. *J. Chem. Phys.* **1993**, *98*, 10089–10092.
- (51) Essmann, U.; Perera, L.; Berkowitz, M. L.; Darden, T.; Lee, H.; Pedersen, L. G. *J. Chem. Phys.* **1995**, *103*, 8577–8592.
- (52) Berendsen, H. J. C.; Postma, J. P. M.; van Gunsteren, W. F.; DiNola, A.; Haak, J. R. *J. Chem. Phys.* **1984**, *81*, 3684–3690.
- (53) Hess, B.; Bekker, H.; Berendsen, J. J. C.; Fraaije, J. G. E. M. *J. Comput. Chem.* **1997**, *18*, 1463–1472.
- (54) Miyamoto, S.; Kollman, P. A. *J. Comput. Chem.* **1992**, *13*, 952–962.
- (55) Rappaport, D. *Mol. Phys.* **1983**, *50*, 1151.
- (56) Dickerson, R. E. *Nucleic Acids Res.* **1989**, *17*, 1797–1803.
- (57) Dickerson, R. E. *Methods Enzymol.* **1992**, *211*, 67–110.
- (58) Lu, X. J.; Olson, W. K. *J. Mol. Biol.* **1999**, *285*, 1563–1575.
- (59) Hassan, M. A. E.; Calladine, C. R. *J. Mol. Biol.* **1998**, *282*, 331–343.
- (60) Young, M. A.; Ravishanker, G.; Beveridge, D. L.; Berman, H. M. *Biophys. J.* **1995**, *68*, 2454–2468.
- (61) Wu, Z.; Ono, A.; Kaianoshio, M.; Bax, A. *J. Biomol. NMR* **2001**, *19*, 361–365.
- (62) Arora, N.; Jayaram, B. *J. Phys. Chem. B* **1998**, *102*, 6139–6144.
- (63) Calladine, C.; Drew, H. R. *J. Mol. Biol.* **1984**, *178*, 773–782.
- (64) Yanagi, K.; Prive, G. G.; Dickerson, R. E. *J. Mol. Biol.* **1991**, *217*, 201–214.
- (65) Varnai, P.; Djuranovic, D.; Lavery, R.; Hartman, B. *Nucleic Acids Res.* **2002**, *30*, 5398–5406.
- (66) Perez, A.; Marchan, I.; Svozil, D.; Sponer, J.; Cheatham, T. E., III; Laughton, C. A.; Orozco, M. *Biophys. J.* **2007**, *92*, 3817–3829.
- (67) Schneider, B.; Neidle, S.; Berman, H. M. *Biopolymers* **1997**, *42*, 113–124.
- (68) Gao, Y.-G.; Robinson, H.; Wang, A. H.-J. *Eur. J. Biochem.* **1999**, *261*, 413–420.
- (69) Pearlman, D. A.; Kim, S. H. *J. Biomol. Struct. Dyn.* **1986**, *4*, 69–98.
- (70) Ryckaert, J. P.; Bellemans, A. *Chem. Phys. Lett.* **1975**, *30*, 123–125.
- (71) Ryckaert, J. P.; Bellemans, A. *Faraday Discuss. Chem. Soc.* **1978**, *66*, 95–106.
- (72) Hartmann, B.; Piazzolla, D.; Lavery, R. *Nucleic Acids Res.* **1993**, *21*, 561–568.
- (73) Tse, W. C.; Boger, D. L. *Chem. Biol.* **2004**, *11*, 1607–1617.
- (74) ElHassan, M. A.; Calladine, C. R. *Philos. Trans. R. Soc. London, Ser. A—Math., Phys. Eng. Sci.* **1997**, *355*, 43–100.
- (75) Olson, W. K.; Zhurkin, V. B. *Curr. Opin. Struct. Biol.* **2000**, *10*, 286–297.
- (76) Goodsell, D. S.; Kaczor-Grzeskowiak, M.; Dickerson, R. E. *J. Mol. Biol.* **1994**, *24*, 79–96.

JP1035663